Explanation for the seam line discontinuity in terrestrial laser scanner point clouds

D.D. Lichti[a], C.L. Glennie[b], K. Al-Durgham[a], A. Jahraus[a], J. Steward[a]

[a] Department of Geomatics Engineering
The University of Calgary
2500 University Dr NW
Calgary AB T2N 1N4
Canada

[b] Department of Civil and Environmental Engineering
University of Houston
4726 Calhoun Road
Houston, TX 77204-4003
USA

Abstract

The so-called seam line discontinuity is a phenomenon that can be observed in point clouds captured with some panoramic terrestrial laser scanners. It is an angular discontinuity that is most apparent where the lower limit of the instrument's angular field-of-view intersects the ground. It appears as step discontinuities at the start (0° horizontal direction) and end (180°) of scanning. To the authors' best knowledge, its cause and its impact, if any, on point cloud accuracy have not yet been reported. This paper presents the results of a rigorous investigation into several hypothesized causes of this phenomenon: differences between the lower and upper elevation angle scanning limits; the presence of a vertical circle index error; and changes in levelling during scanning. New models for the angular observations have been developed and simulations were performed to independently study the impact of each hypothesized cause and to guide the analyses of real datasets. In order to scrutinize each of the hypothesized causes, experiments were conducted with seven real datasets captured with six different instruments: one hybrid-architecture scanner and five panoramic scanners, one of which was also operated as a hybrid instrument. This study concludes that the difference between the elevation angle scanning limits is the source of the seam line discontinuity phenomenon. Accuracy assessment experiments over real data captured in an indoor test facility demonstrate that the seam line discontinuity has no metric impact on the point clouds.

1.0 Introduction

This paper addresses the discontinuity that can be observed between the start and end of a point cloud captured with some terrestrial lasers scanners (TLSs), specifically those having panoramic architecture (Staiger, 2003). The seam line mismatch is an angular discontinuity in the data and that is most apparent at the location where the lower limit of the instrument's field-of-view (FoV) intersects the ground. For an ideal, levelled instrument, the intersection of the lower FoV and a horizontal plane defines

a circle. As a result of the seam line discontinuity, this FoV boundary deviates from the ideal, circular shape. Step discontinuities exist at diametrically-opposed locations, nominally at horizontal directions of 0° and 180°. Examples from two levelled instruments at a height of 1.25 m above a laboratory floor are shown in Fig. 1. Two questions that naturally arise are:

1. What is the cause of this discontinuity?
2. Does this discontinuity adversely affect the accuracy of the point cloud?

Identifying the exact cause of such an artefact can be challenging due to the lack of precise knowledge about instrument internal architecture and measurement procedures. Such details are generally regarded as proprietary information and, hence, not available to users. Quantification of the effect on the metric quality of point cloud data—if any—is important, even if the magnitudes of the discontinuity examples in Fig. 1 appear to be small. The linear equivalent impact of angular errors grows with range, so at 10 m the discrepancies shown would be on the order of centimetres.

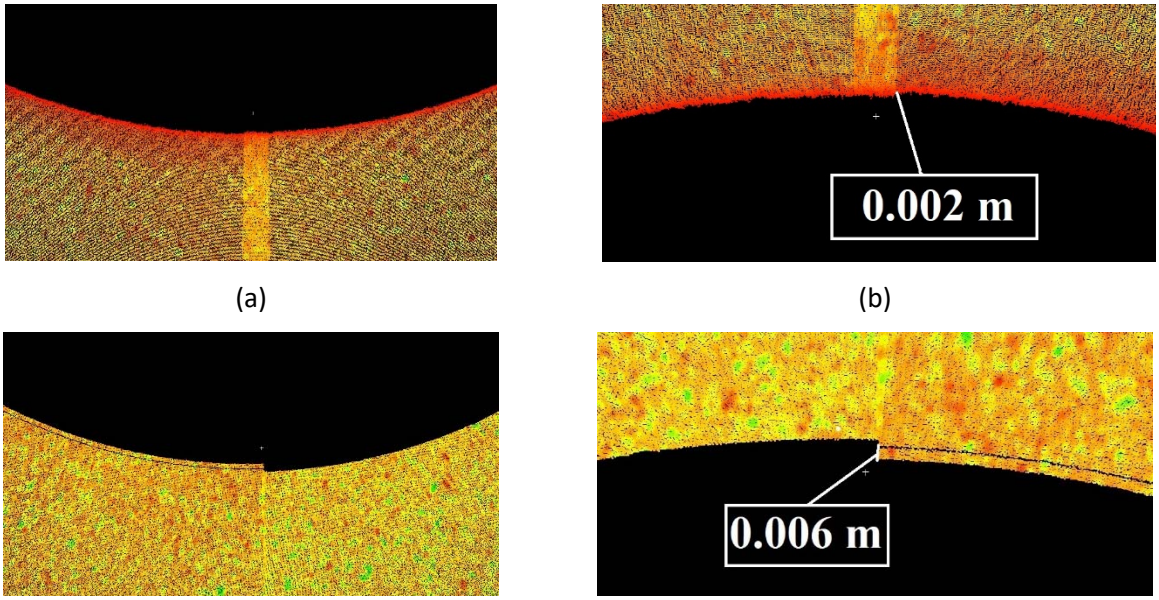

(a) (b)

(c) (d)

Fig. 1. Seamline mismatch examples at a) 0° and b) 180° for a Leica HDS6100 and at c) 0° and d) 180° for a Z+F Imager 5010.

Al-Manasir and Lichti (2015) report the existence of the discontinuity or seam line mismatch in point clouds in their calibration study of a Leica HDS7100 instrument. Discussion about the existence of the problem can also be found in online forums. However, to the authors' best knowledge, detailed scientific investigation into the underlying cause and effect has not been reported. The current study proposes that at least three possible causes can be identified: unequal lower and upper angular scanning

limits; the presence of a vertical circle index error; and the instrument going off level during data acquisition.

The angular scanning limits are internally-defined parameters that mark the start and end of range measurement collection within each vertical profile. These are discussed in detail in the next section. The vertical circle index error is an instrumental systematic error that can exist in terrestrial laser scanners. The error occurs when the origin of elevation angle measurements does not lie in the horizontal plane of the instrument's internally-defined co-ordinate system or, equivalently, when the origin of zenith angle measurements does not coincide with the instrument's vertical axis. It can be estimated by self-calibration performed with redundant observations of a target field collected in well-designed network (e.g., Lichti, 2007; Medić et al., 2017; Reshetyuk, 2010).

Several reports exist in the literature of varying methods and quality of tilt compensation used in terrestrial laser scanners that justify the plausibility of the third hypothesis. Kersten et al. (2009) tested six TLS instruments from five different manufacturers. All were equipped with inclination sensors. They report that the acquired data can be corrected in different ways. Whereas some instruments correct data during data collection, others do so once scanning has finished. They found that while the tilt compensation was very effective for some instruments, significant errors remained in the data captured with others. Silvia and Olsen (2012) investigated the stability of TLS inclination sensors by testing four scanners, each from a different manufacturer. They report that the inclination sensors are effective when used properly. Moreover, compensators are not able to reach vertical equilibrium during fast scans. Consequently, if an instrument goes off level, the compensation of the tilt error may not be sufficient. Hartzell et al. (2015) demonstrate the application of inclination sensor observations for the correction of scanner data in order to compensate for the settling of a Riegl instrument. They found the inclination measurements to be corrupted with a high degree of random noise. Accordingly, low-pass filtering was necessary for the effective reduction of levelling errors.

This work reports the results of a detailed investigation into possible causes of the seam line discontinuity. New angular observation models are first presented in order to better facilitate analysis of the effect. Simulations are conducted to demonstrate the effect of each hypothesized cause of the seam line discontinuity and to guide the analyses of real data. Controlled experiments have been designed and performed on several different TLS instruments in order to identify the cause of the effect and to quantify its impact, if any. Finally, the experimental results are presented and interpreted and conclusions are drawn.

2.0 Methodology

2.1 Angular Observation Models

Consider a panoramic TLS instrument having its right-handed scanner space (xyz) origin located at C in Fig. 2. Strictly speaking, the scanner system need not be levelled with respect to an external, right-handed object space coordinate system, UVW, but it will assumed to be at this stage. The instrument rotates about the z axis in discrete steps through 180°, collecting range measurements in approximately vertical profiles at each horizontal increment. The horizontal direction observation, θ, can be expressed in terms of the Cartesian scanner-space co-ordinates as follows:

$$\theta = \arctan\left(\frac{y}{x}\right) \tag{1}$$

Equation (1) is relevant for some instruments used in this work, specifically the Faro Focus 3D (Lichti, 2007). For other instruments, such as the Leica HDS6100 and the Zoller+Fröhlich Imager 5010 (Al-Manasir and Lichti, 2015), the horizontal direction is given by

$$\theta = \arctan\left(\frac{x}{-y}\right) \tag{2}$$

In either case, the allowable range is $0° < \theta \leq 180°$ (Lichti, 2010). The upper limit of this range is 360° for panoramic scanners that complete a full revolution about the vertical axis and collect data on two faces. For hybrid scanners, either equation may be applicable but the range is $0° < \theta \leq 360°$.

Within a vertical profile, range measurements are collected in nominally equal increments of arc. The elevation angle observation, α, can be parameterized as per Equation 3. The allowable range for panoramic scanners is defined to be $-90° < \alpha \leq 270°$, though the exact limits span a lower angular range, as described in greater detail in the next sub-section. The allowable range for hybrid scanners is $-90° \leq \alpha \leq 90°$. Again, the exact limits may be lower. These angle definitions follow those reported in (Abbas et al., 2014; García-San-Miguel and Lerma, 2013; Lichti, 2007). Other formulations are also reported (Medić et al., 2017; Muralikrishnan et al., 2015; Reshetyuk, 2010).

$$\alpha = \arctan\left(\frac{z}{\sqrt{x^2 + y^2}}\right) \tag{3}$$

The laser scanning mechanism can be further parameterized to describe any deviations from the ideal ranges of the observed angles θ and α. Accordingly, two new angles are defined in order to investigate the cause of the seam line mismatch and to quantify its impact. The first, γ, is a vertical angle

referenced to the negative z-axis rather than the rotating line used for elevation angle, α (c.f. Fig. 2) and is computed as per Equation 4. The second, ψ, is a horizontal angle computed as per Equation (1) or (2) but, unlike θ, its allowable range is $-180° < \psi \leq 180°$.

$$\gamma = \arctan\left(\frac{\sqrt{x^2 + y^2}}{-z}\right) \tag{4}$$

For the sake of completeness, it is worth noting that that the range observation, ρ, is defined as

$$\rho = \sqrt{x^2 + y^2 + z^2} \tag{5}$$

and the relationship between scanner space and object space is given by the rigid body transformation

$$\begin{pmatrix} x \\ y \\ z \end{pmatrix}_{ij} = \mathbf{M}_j \left(\mathbf{r}_i - \mathbf{r}_j^c\right) \tag{6}$$

where $\mathbf{M}_j$ is the rotation matrix of scan j; $\mathbf{r}_i$ is the object space position vector of scanned point i; and $\mathbf{r}_j^c$ is the object space position vector of scan j.

With the new angular observation models defined, instrument operation in terms of angular data collection can be investigated in detail. The analysis starts for a panoramic-architecture instrument having equal scanning limits and that is unaffected by systematic errors. The cases of unequal scanning limits, the presence of a vertical circle index error and the instrument going off level during scanning are then introduced. Finally, the ideal hybrid case is presented with discussion of scanning limits and the vertical circle index error for completeness.

2.2 Panoramic Scanner Data Collection

In panoramic instrument data collection, all points in the vertical profile passing through H are assumed to have the same horizontal direction, θ_H (Fig. 2). Within the vertical profile, range measurements are collected from the lower elevation angle limit, α_L, denoted by point L, through zenith, Z, and down to the upper elevation angle limit, $\alpha_{L'}$, denoted by point L'. The origin of the elevation angle measurements is the rotating line CH, which lies in the xy plane. Ideally, the acute angles between the z axis and lines CL and CL' , $\gamma_{L'}$ and $\gamma_{L'}$, respectively, are equal. Since $\alpha_L < 0°$ by definition, the elevation angle limits satisfy the relationship $\alpha_{L'} = 180° - \alpha_L$. Thus, the intersection of the elevation angle limits (α_L and $\alpha_{L'}$) and the scanner-space horizontal plane passing through O below the instrument—the edge of the FoV—is a circle.

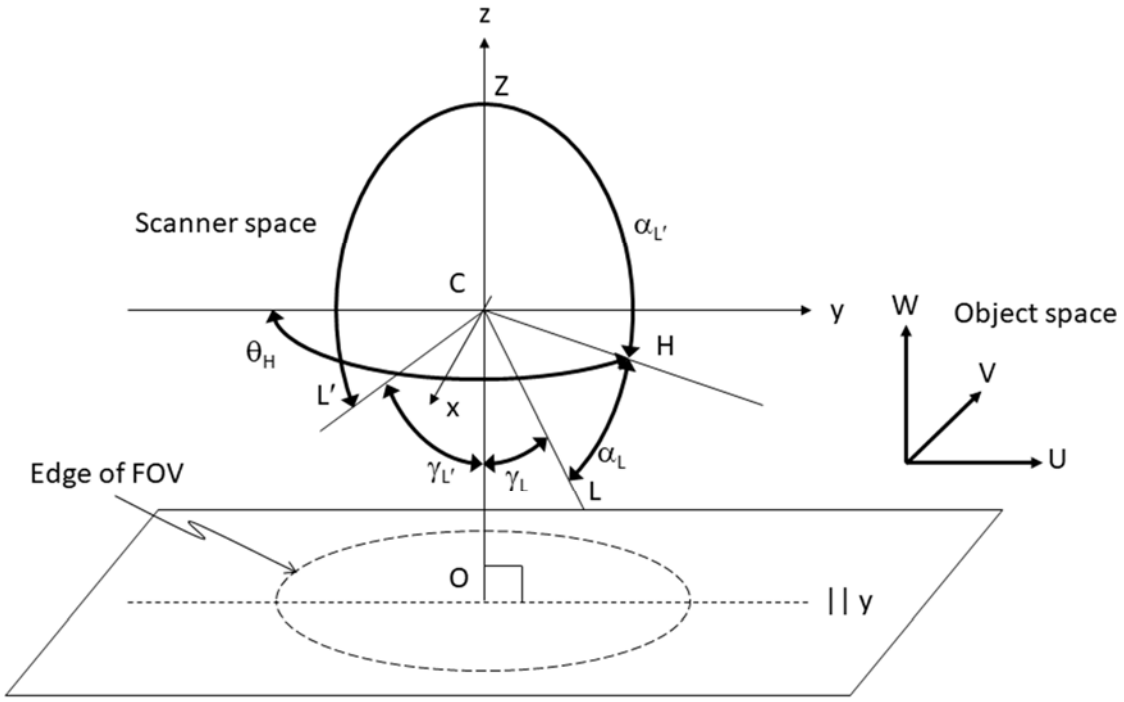

Fig. 2. Panoramic TLS instrument data collection.

2.3 Panoramic Scanner—Differing Elevation Angle Limits

The situation where the lower and the upper angular scanning limits differ is depicted in Fig. 3. In this case the γ angles are not equal, i.e. $\gamma_L \neq \gamma_{L''}$, and the elevation angle limits do not satisfy the same relationship: $\alpha_{L''} \neq 180° - \alpha_L$. The intersection of the elevation angle limits, α_L and $\alpha_{L''}$, and the horizontal plane passing through O is two semi-circles of different radii on either side of the y axis. The magnitude of the discontinuity is $\delta\alpha = \alpha_{L''} + \alpha_L - 180°$.

Range measurements are collected at (nominally) equal increments of elevation angle starting from the lower limit. If the lower and upper limits are symmetric about the z-axis, then uniform angular sampling within the profile is symmetric about the z-axis (Fig. 4a). In this case, the seam line discontinuity does not exist. If the limits are unequal, then the sampling structure within a vertical profile is offset, so the sampling within the profile is asymmetric about the z-axis (Fig. 4b). The discontinuity in the sampling pattern at the seam line exists throughout the profile, but it is most apparent at the edge of the FoV. In principle, it should not affect the accuracy of the collected point coordinates.

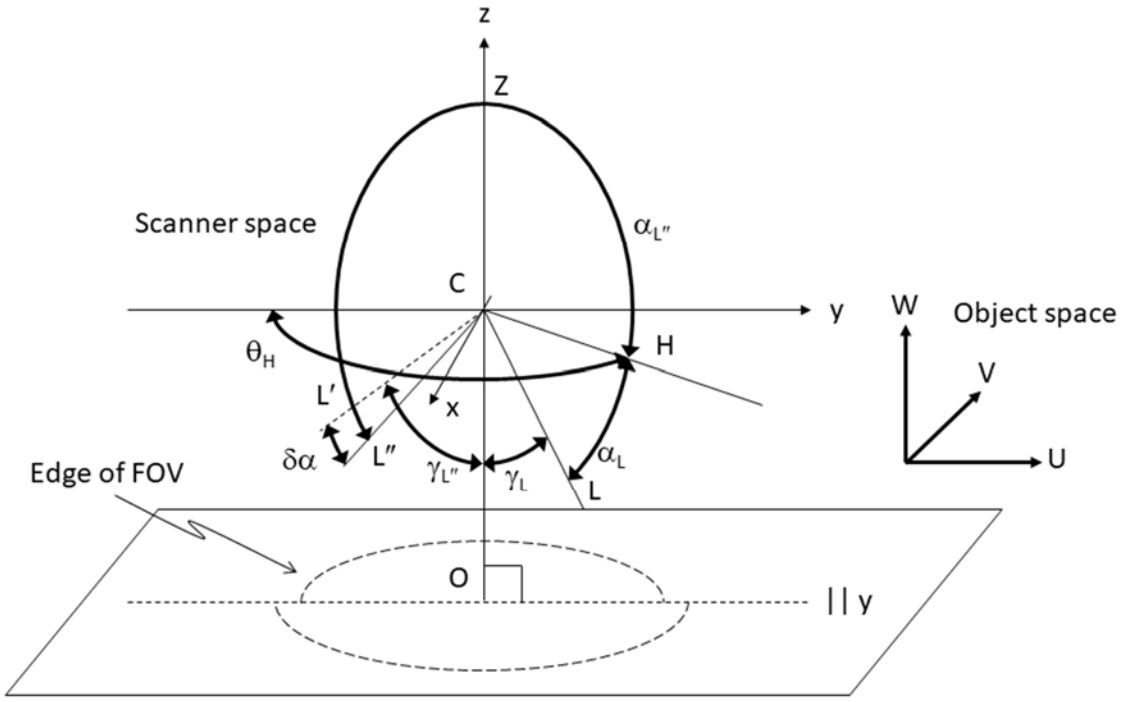

Fig. 3. Panoramic TLS instrument data collection with differing lower and upper angular scanning limits.

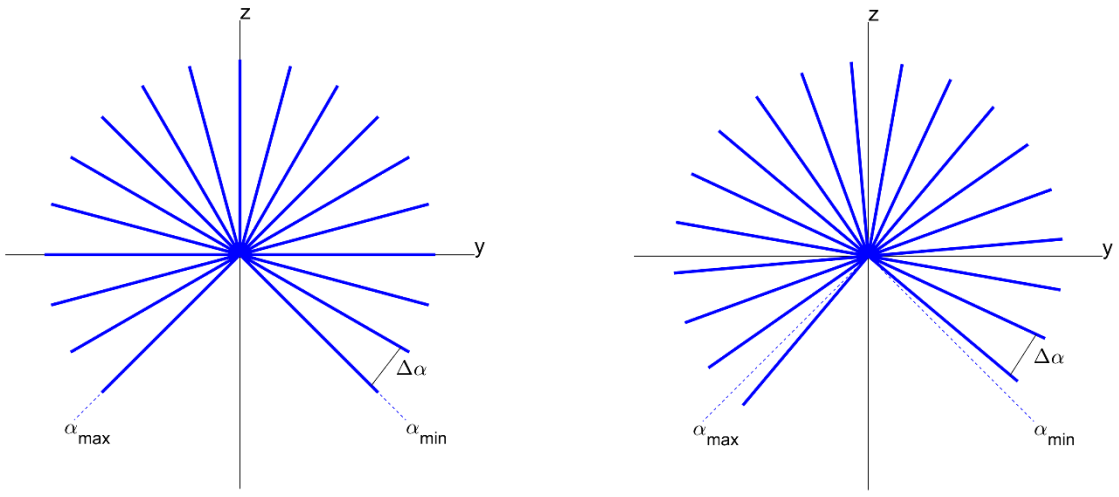

(a) (b)

Fig. 4. Panoramic TLS vertical profile sampling with a) equal lower and upper limits and b) unequal limits

2.4 Panoramic Scanner—Vertical Circle Index Error

Fig. 5. depicts the case where the instrument possesses a vertical circle index error. The reference for the elevation angle measurements is not CH, but CH′ due to the vertical circle index error, c_0. The

intersection of the elevation angle limits, α_L and $\alpha_{L'}$, and the horizontal plane passing through O is two semi-circles of different radii on either side of the y axis. The magnitude of the angular difference is $2c_0$ since the elevation angles at L and L′ are both biased, that is $\alpha_{L'} = 180° - \alpha_L + 2c_0$ and $\gamma_L \neq \gamma_{L'}$.

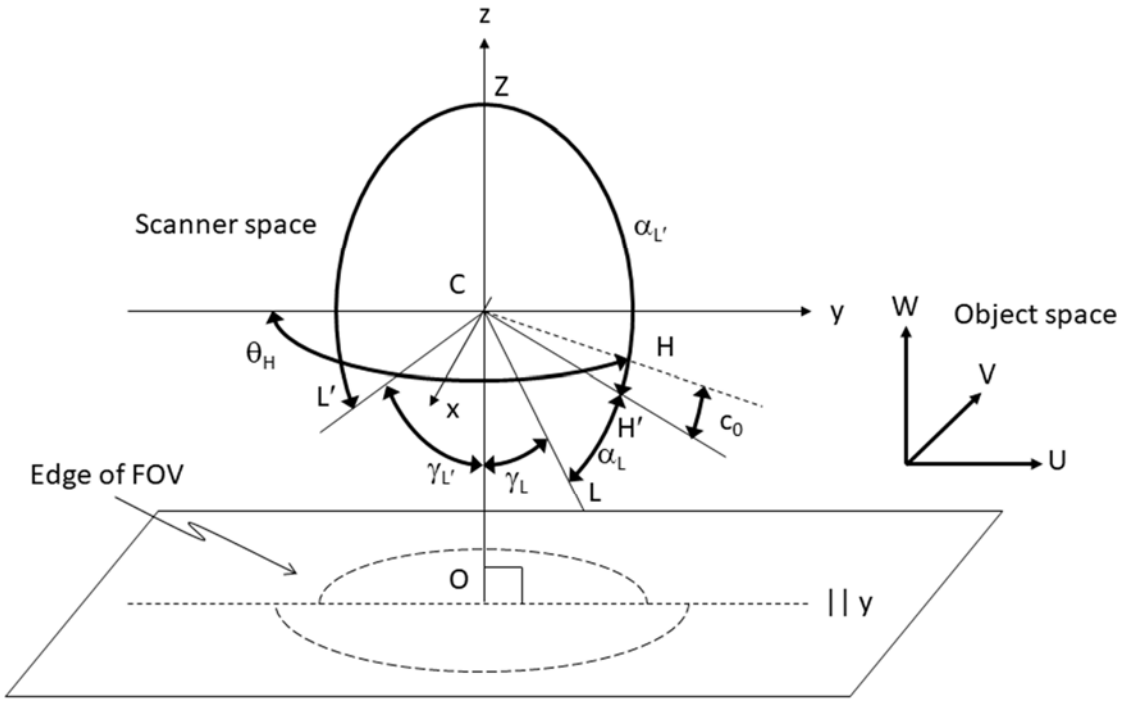

Fig. 5. Panoramic TLS instrument data collection with vertical circle index error.

2.5 Panoramic Scanner—Instrument Goes Off Level During Scanning

Pictured in Fig. 6 is the situation where the TLS instrument goes off level during scanning. In this case, the orientation of the vertical axis, z′, is time dependent. When the instrument is initially levelled and at rest, z′ is vertical and is coincident with the z axis. As the instrument starts to scan, the z′ axis begins to deviate from the z axis. The amount by which it is off level increases as the rotation about the vertical axis increases.

Since the vertical angles are referenced to the internal instrument system, the tilted x′y′z′ system, the acute angles between the - z′ axis and L and the -z′ axis and L′ are equal. However, the corresponding angles referenced to the -z axis, i.e. the normal to the object space horizontal plane, are not, that is $\gamma_L \neq \gamma_{L'}$. When projected onto the horizontal plane, the lower edge of the FoV traces out a curve of changing radius that results in the discontinuities at 0° and 180°.

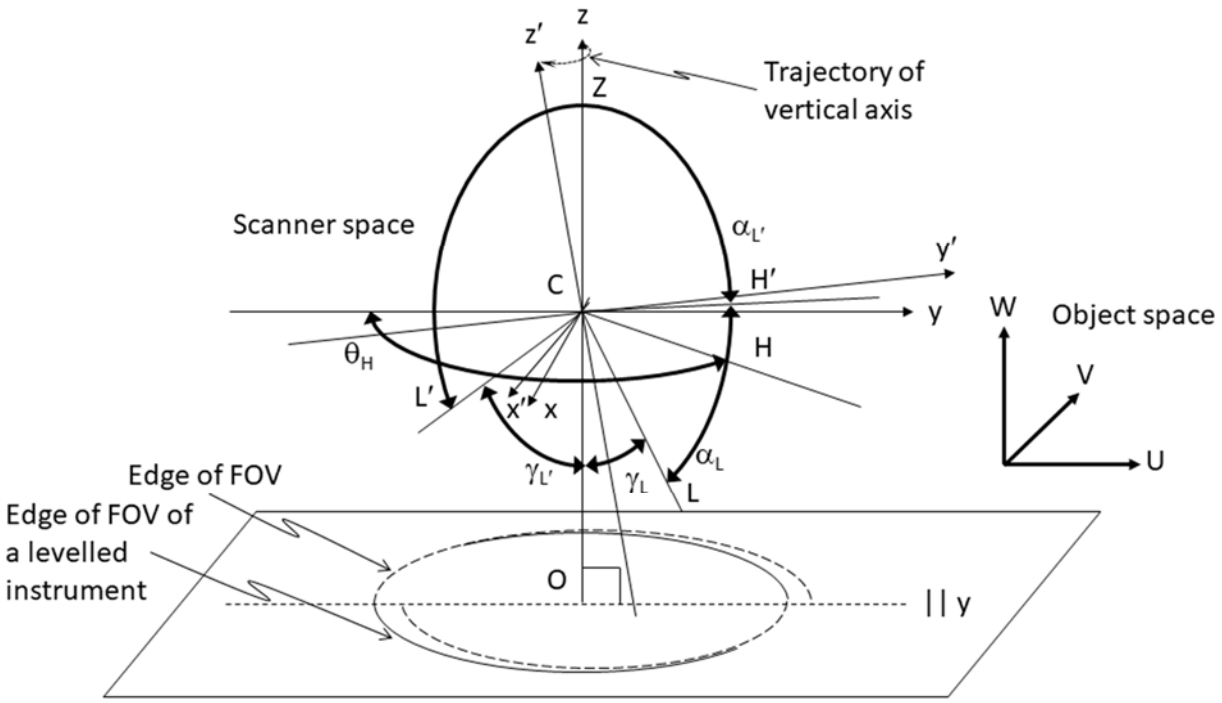

Fig. 6. Panoramic TLS instrument data collection when instrument goes off level during scanning

2.6 Hybrid Scanner Data Collection

A hybrid TLS instrument (Fig. 7) collects data by rotating about the z axis through 360°. The upper limit of scanning, L′, is at zenith, Z. L′ may deviate from Z due to the vertical circle index error. The intersection of the elevation angle limit (α_L) and the horizontal plane passing through O below the instrument is a circle since the scanner rotates through 360° about its vertical axis, regardless of the upper limit and regardless of whether a vertical circle index error exists. Thus, the angle γ_L is invariant to horizontal direction and so no discontinuity should exist at the edge of the FoV as long as the instrument remains level.

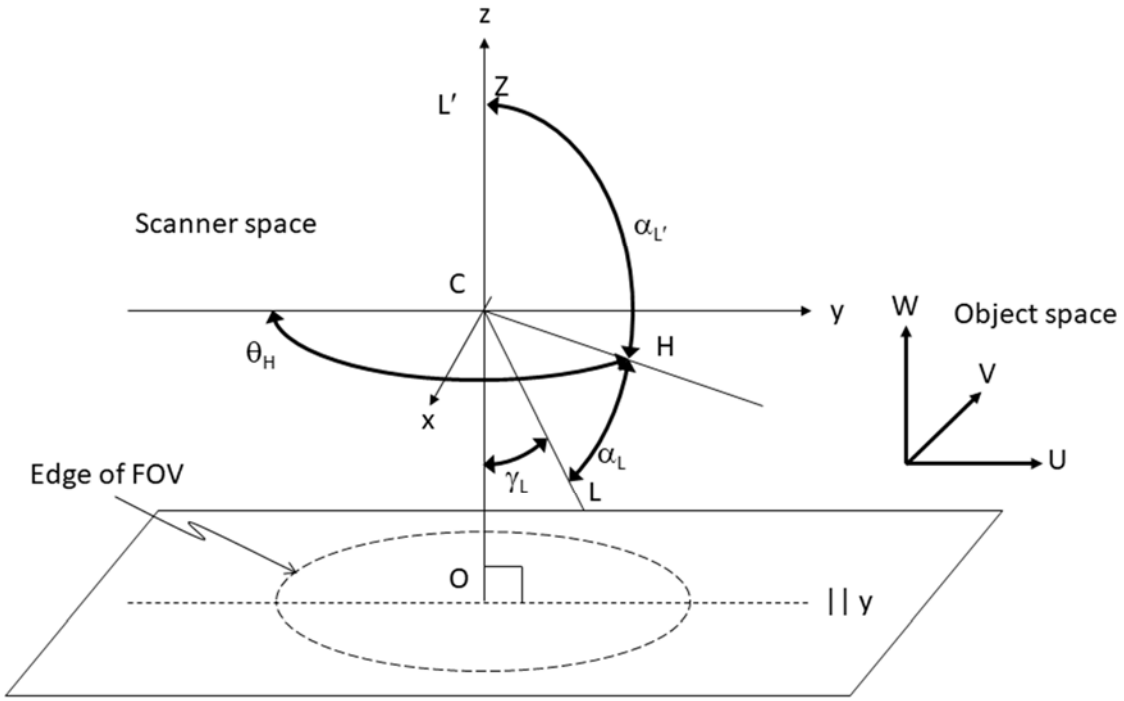

Fig. 7. Hybrid TLS instrument data collection.

2.6 Panoramic Scanner Data Simulation

To illustrate the effect of the three hypothesized causes of the seam line discontinuity, a series of simulations was performed. Panoramic instrument data were generated with a uniform sampling interval of 0.1° in both θ and α (Fig. 8) and nominal elevation angle limits of -45° and 225°. An arbitrary angular error of 0.08° was introduced to illustrate four different effects in terms of γ as a function of the full 360° range of horizontal direction, ψ. Two cases for which the instrument was assumed to be levelled are presented: different elevation angle limits and the presence of a vertical circle index error. As described, both sources cause a similar effect: discontinuities at ψ = 0° and 180° but with respective magnitudes of 0.08° and 0.16°. It is important to note that whereas the presence vertical circle index error introduces a bias in the point cloud, differing angular scanning extents does not.

Two un-levelled cases are also presented. In the first, the instrument levelling error is constant during scanning, whereas in the second it is level at the start of scanning but goes off level in proportion to the horizontal direction scanning angle. The constant levelling error case gives rise to a sinusoidal pattern as expected (Chow et al., 2013; Lichti et al., 2011; Ogundare, 2015). This error is of no metric consequence to the point cloud if the instrument tilt angles are estimated in registration or self-

calibration. It is presented here for reference to aid in the interpretation of the real data results. In the final case, the sampling pattern exhibits two discontinuities and is periodic, but is not a pure sinusoid.

The ψ-γ plots can be used to identify the existence of a discontinuity. However, a dataset possessing two or more of the presented effects requires additional analyses. Self-calibration can be used to estimate the vertical circle index error. Subsequent analyses of the corrected data can then identify if a residual discontinuity exists in the ψ-γ plot, which would suggest differing angular scanning limits. Moreover, the constant levelling error can be compensated by the estimated orientation angles in the self-calibration solution. Following data correction, the ψ-γ plot can be analysed for the presence of a linearly-increasing levelling error.

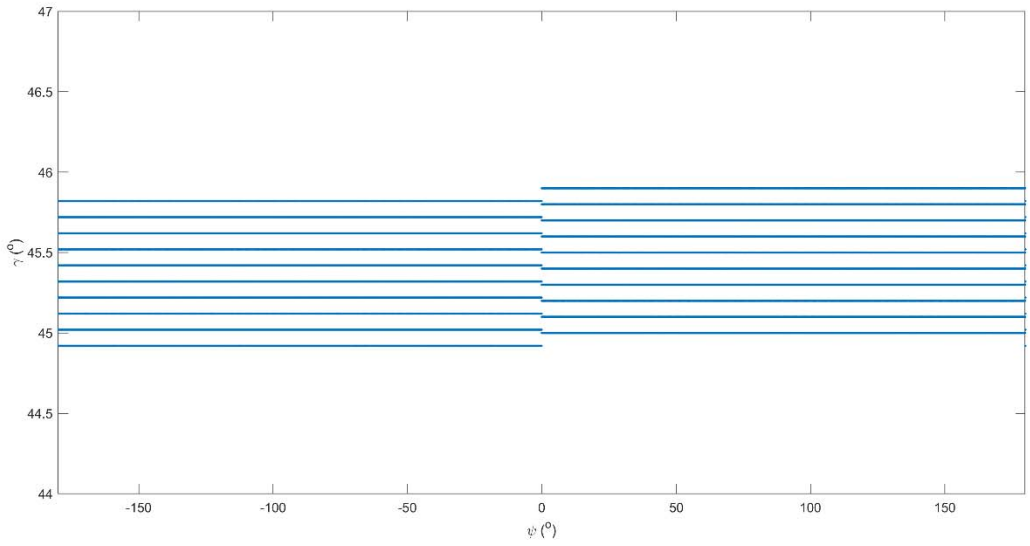

(a)

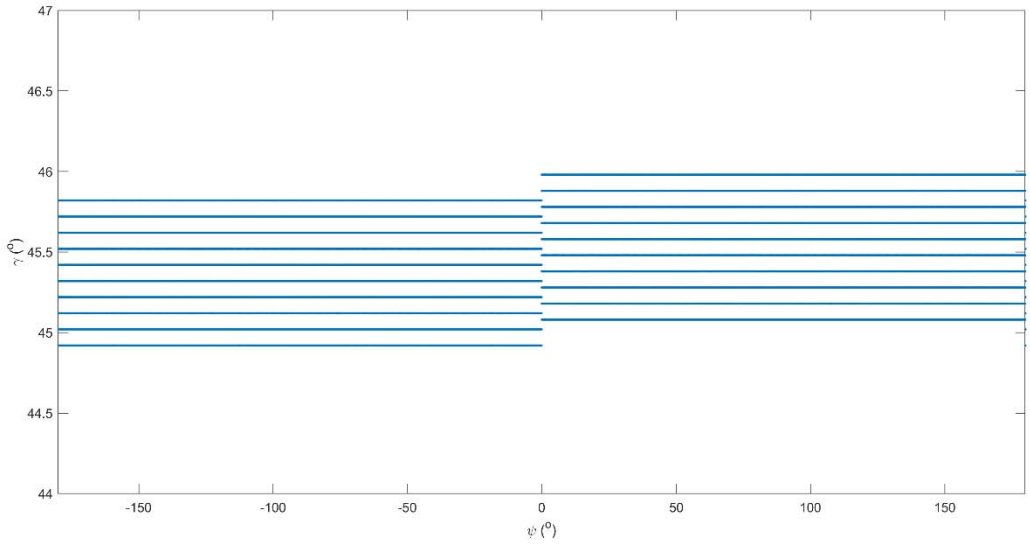
47
46.5
46
45.5
45
44.5
44
-150
-100
-50
0
50
100
150
γ (^{o})
ψ (^{o})

(b)

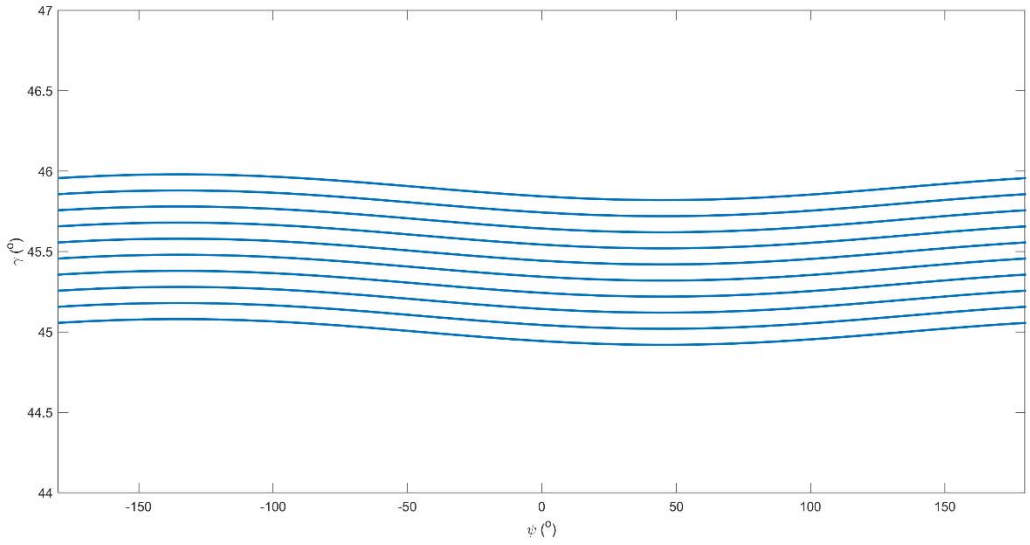
47
46.5
46
45.5
45
44.5
44
-150
-100
-50
0
50
100
150
γ (^{o})
ψ (^{o})

(c)

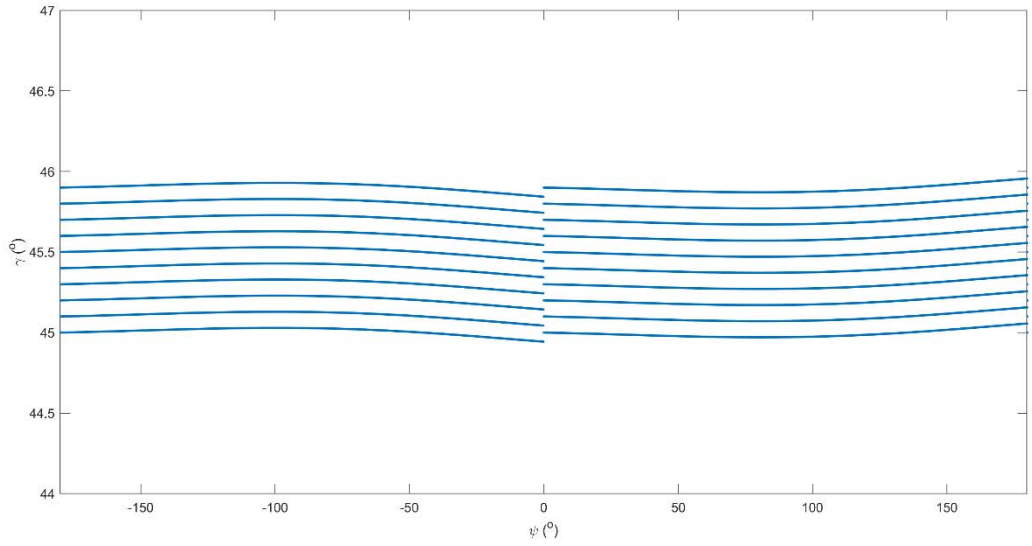

(d)

Fig. 8. γ vs ψ for a) lower and upper angular scanning limits that differ by 0.08°, b) the presence of a 0.08° vertical circle index error, c) constant levelling error of 0.08°, and d) linearly increasing levelling error from 0° at θ=0° to 0.08° at θ=180°.

3.0 Experiment

An experiment to test the presented hypotheses of the cause of the seam line discontinuity has been designed and executed. Several TLS instruments were tested in the 10.0 m x 9.0 m x 4.3 m calibration room described in Lichti et al. (In Press). Each scanner was mounted in a tribrach on a heavy tripod for data capture. The tripod was rigidly affixed to the floor and the instrument levelled prior to scanning. Nine scans were captured with each instrument from three different locations throughout the room. The orientation was changed for each successive scan by rotating the instrument about its z axis by 120° in order to de-correlate the exterior orientation parameters and additional parameters (APs).

Six different scanners from four different manufacturers were tested. Five of the instruments are panoramic and one is hybrid. One panoramic instrument, the Leica HDS6100, can also be operated as a hybrid scanner. Accordingly, two datasets were collected with this instrument. In this investigation, the most pertinent instrumental details are the architecture and the means available to sense and compensate for instrument tilt (Table 1).

A total of 200 purpose-built Compact Disc targets were mounted on the floor, ceiling and the walls of the room. The target design and the associated algorithm for measuring the co-ordinates of their centres from the point clouds are described in Lichti et al. (In Press). The maximum range observed in the

laboratory was 10.5 m. The experiment was performed in a closed, temperature-controlled room at the University of Calgary. Environmental conditions were assumed to be constant during data capture.

Two sets of data analyses were performed. First, the relationship between the auxiliary horizontal direction angle, ψ, and the auxiliary vertical angle, γ, was analyzed at the floor-FoV boundary for all nine scans collected with each instrument. The simulation results for the different effects were used as templates to identify patterns visible in the real γ-ψ plots.

Second, a minimally-constrained, self-calibrating bundle adjustment (Lichti, 2007) was performed on each dataset. Self-calibration estimates the six exterior orientation parameters for each scanner location, all target centre co-ordinates and the APs of instrumental systematic error models. Known systematic effects were modelled by stepwise model construction using graphical and statistical tools. Incidence angle thresholds were applied and observations to low-contrast targets were removed as per the findings reported in Lichti et al. (In Press).

Accuracy assessment was conducted by comparing the scanned co-ordinates of sixty-one check point targets estimated by self-calibration with independently-surveyed co-ordinates. A high-precision survey was conducted with a Leica TS30 total station and precision scale bar to estimate the check point co-ordinates. The mean precision at the 95% confidence level was 1.1 mm in each planar dimension and 0.3 mm in the vertical dimension.

Table 1. Scanners used in the experiment and manufacturer-provided tilt/inclination sensing/compensation information.

Instrument	**Architecture**	**Tilt/inclination sensing/compensation**
Faro Focus 3D #1 Faro Focus 3D #2[1]	Panoramic	Dual axis compensator: Levels each scan with an accuracy of 0.015° and a range of ±5° Data must be re-acquired if the instrument goes off level during scanning
Leica HDS6100[2]	Panoramic Can also be operated as a Hybrid scanner	Sensor detects instrument tilt and compares values recorded at the beginning and the end of a scan. Is not a compensator. Resolution: 0.001° = 1/1000° Relative accuracy: 0.002° = 1/500°

		Working range: ≅±2.5°
Leica P40[3]	Panoramic	Dual-axis compensator: Liquid sensor with real-time onboard compensation; selectable on/off Resolution 1", Dynamic range ± 5' Accuracy 1.5"
Riegl VZ-400[4]	Hybrid	On-board, integrated inclination sensors Tilt range: ±10° Typical accuracy: ±0.008°
Zoller and Fröhlich Imager 5010[5]	Panoramic	Dual-axis compensator. The Dynamic Compensator will correct angular tilt for each pixel during scan acquisition. Selectable on/off Resolution: 0.001° Measurement range: ±0.5° Accuracy: < 0.007°

[1] FARO Technologies, 2013. FARO Focus^{3D} Features, Benefits & Technical Specifications.
[2] Leica Geosystems, 2009. Leica HDS6100: Latest generation of ultra-high speed laser scanner
[3] Leica Geosystems, 2019. Leica ScanStation P30/P40: Because every detail matters
[4] RIEGL Laser Measurement Systems, 2017. RIEGL VZ-400
[5] Zoller + Fröhlich, ND. Z+F IMAGER® 5010XC.

4.0 Results

4.1 Floor- FoV Boundary

Plots of γ vs ψ at the floor-FoV boundary are shown in Fig. 9. The boundary is located at the bottom of the plots. Ideally, the relationship between γ and ψ at the boundary should be constant without any discontinuity. This is true for the two hybrid scanners, the VZ-400 (Fig. 9e) and the second (hybrid) HDS6100 dataset (Fig. 9g), as predicted. Despite the reduced density at the boundary, the trend is nonetheless constant in the HDS6100 data.

Seam-line discontinuities are visible for all five of the panoramic scanners at two values of ψ (Figs. 9a-d, f). In four of the cases the discontinuity occurs at 0° and 180°. It is not known why they occur at approximately -34° and 146° for the P40. The discontinuities range in magnitude from 44″ to more than 19′, which at a range of 10 m project to 2 mm and 56 mm, respectively. While the former effect may not be of great concern in many applications, it would be for deformation monitoring applications where millimetre-level accuracy is sought. This underscores the need to determine the cause of the discontinuity.

The repeatability of the manual measurements of the discontinuity magnitude is high, at 4″ for the Leica instruments (Figs. 9c, d), 8″ for the Faro scanners (Figs. 9a, b) and 20″ for the Imager 5010 (Fig. 9f). In four cases, a pure sinusoidal trend with 360° period is evident. This is due to the standing axis of instrument being slightly off vertical after initial levelling. In contrast, the constant trends on either side of the discontinuity at 0° indicate that the Imager 5010 (Fig. 9f) was levelled.

Despite the presence of angular discontinuities in five of the datasets, there is no evidence of the quasi- sinusoidal trend (c.f. Fig. 8d) that would suggest the instrument levelling changed during data acquisition. If the instrument were going off level during scanning, it is unlikely that it would do so with the same magnitude and in the same direction for all nine scans. Thus, the high repeatability of the discontinuities suggests that there were no levelling problems. There is also no evidence of the levelling changing in the two hybrid datasets (Figs. 9e, g). In addition, instrument levelling was checked before and after scanning and in none of the cases was it observed to have changed. As a result, changes in the levelling during the scanning process can be ruled out as a cause of the seam line discontinuity. To further support this observation, height relative to the scanner system origin as a function of angular direction, ψ, in the vicinity of the seam line discontinuity is plotted for each dataset in Fig. 10. None of the cases exhibits a discontinuity in height that would suggest the presence of a bias due to change in levelling or other systematic effect.

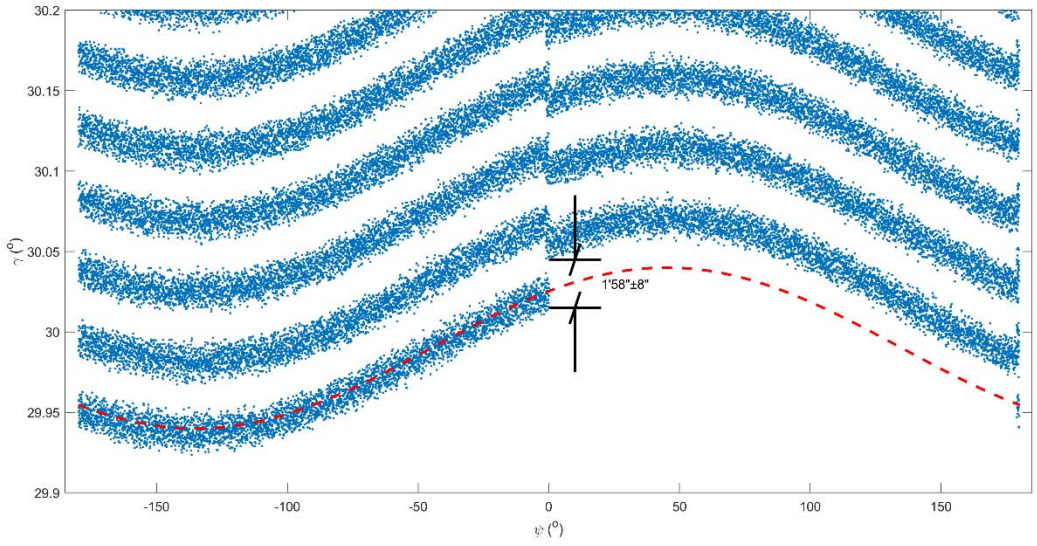

(a)

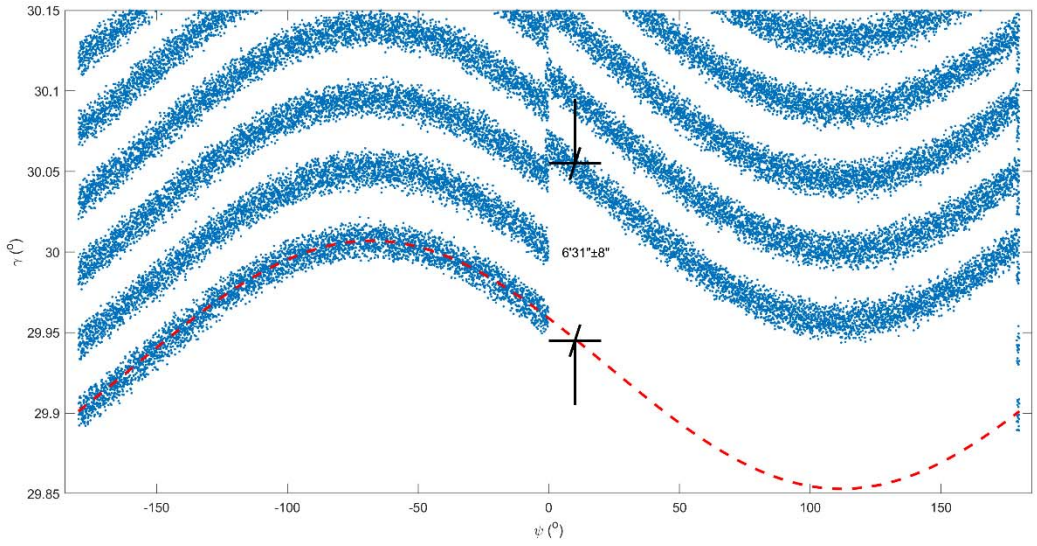
30.15
30.1
30.05
30
29.95
29.9
29.85
γ (°)
6'31"±8"
-150
-100
-50
0
50
100
150
ψ (°)

(b)

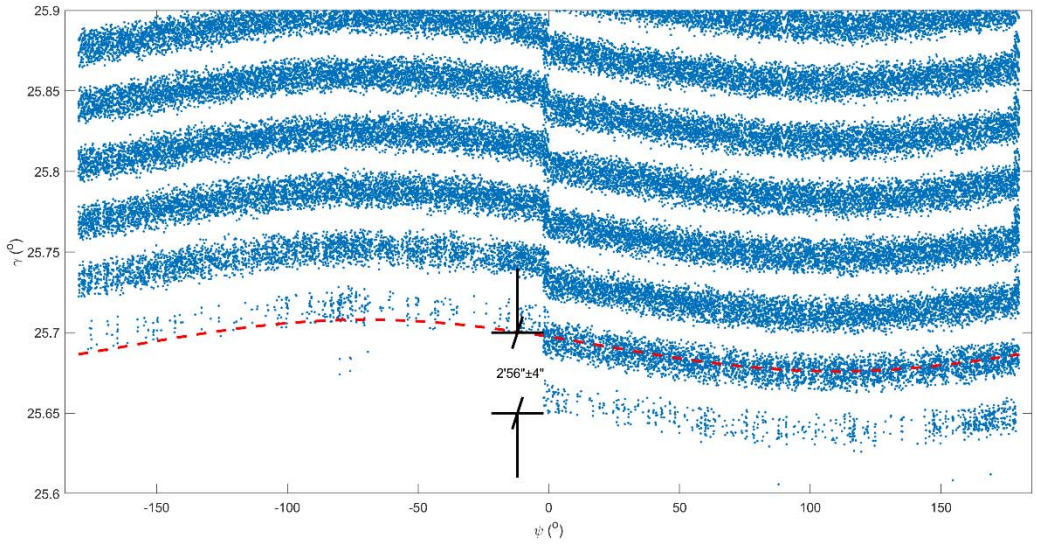
25.9
25.85
25.8
25.75
25.7
25.65
25.6
γ (°)
2'56"±4"
-150
-100
-50
0
50
100
150
ψ (°)

(c)

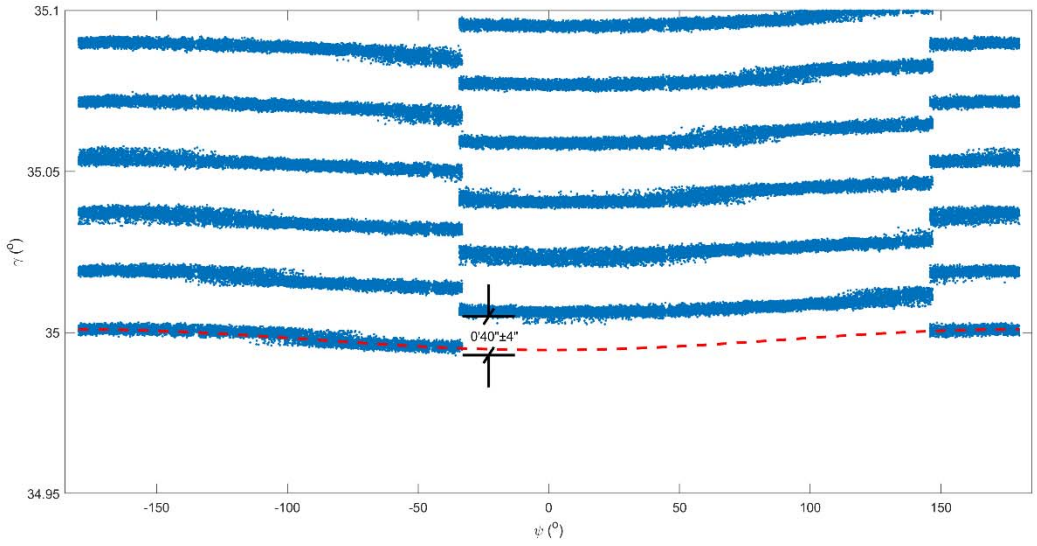
35.1
35.05
35
34.95
γ (°)
0'40"±4"
-150
-100
-50
0
50
100
150
ψ (°)

(d)

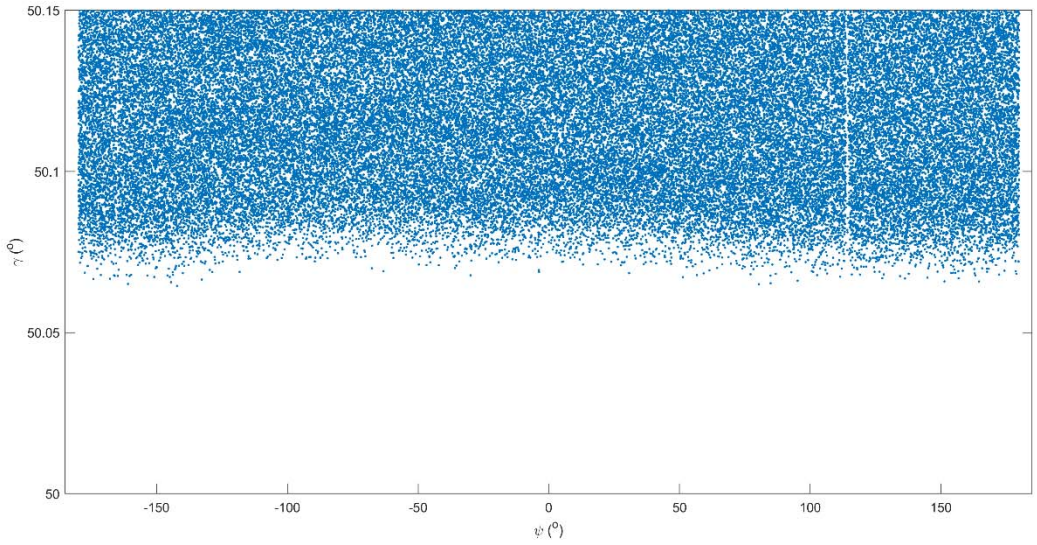
50.15
50.1
50.05
50
γ (°)
-150
-100
-50
0
50
100
150
ψ (°)

(e)

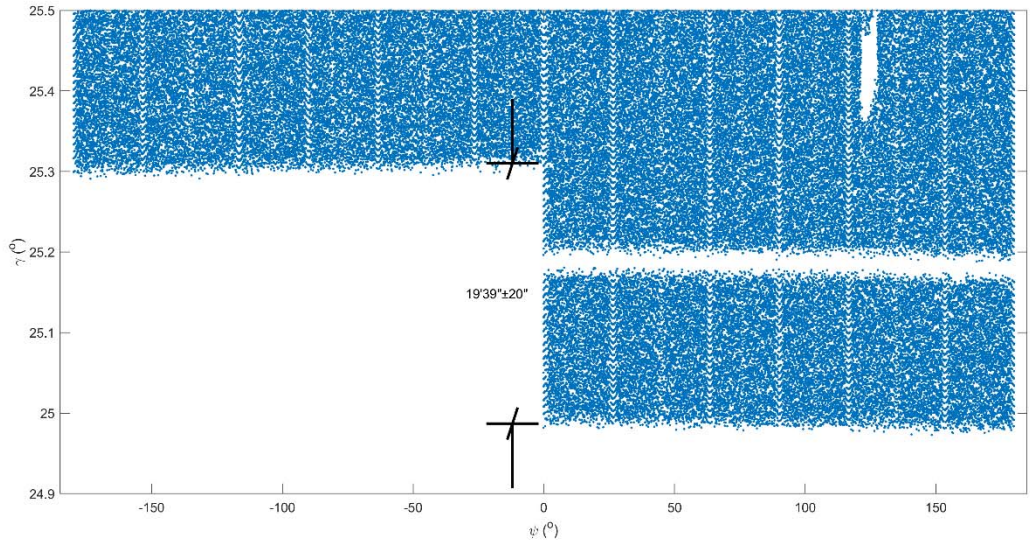

(f)

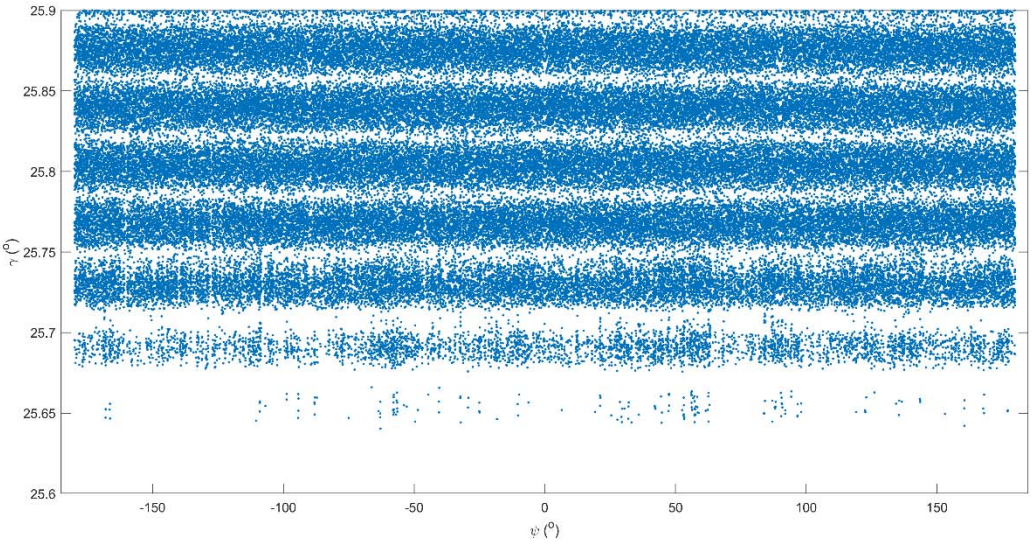

(g)

Fig. 9. Angular scan data (γ vs. ψ) at the floor-FoV boundary: a) Faro Focus 3D instrument 1, b) Faro Focus 3D instrument 2, c) Leica HDS6100 (panoramic mode), d) Leica P40, e) Riegl VZ-400, f): Z+F Imager 5010, g) Leica HDS6100 (hybrid mode). Sinusoidal trends are indicated in cases with initial levelling bias. Measured angular offsets at the seam lines are indicated with standard deviations (computed from nine scans) in all panoramic cases except the VZ-400.

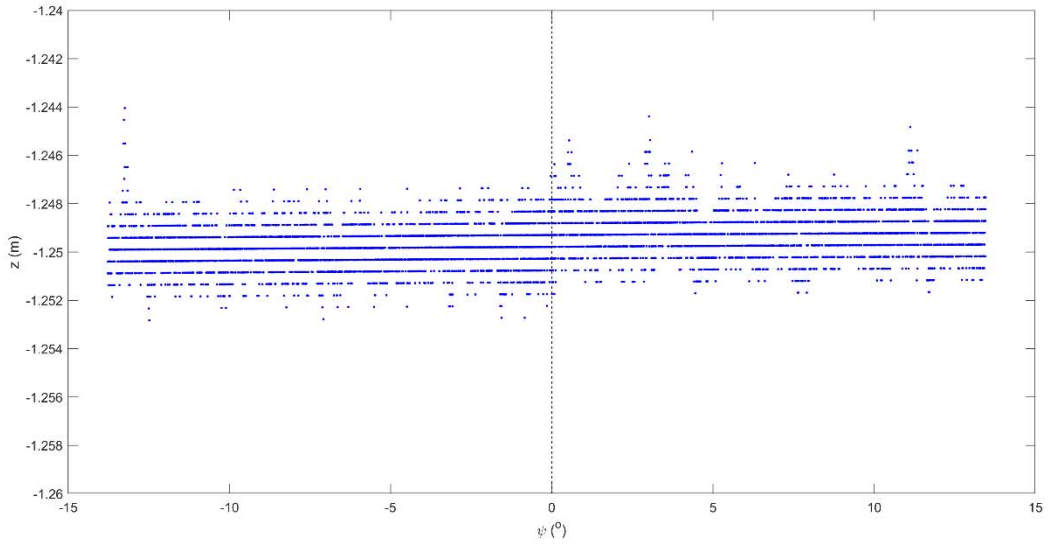
-1.24
-1.242
-1.244
-1.246
-1.248
-1.25
-1.252
-1.254
-1.256
-1.258
-1.26
z (m)
-15
-10
-5
0
5
10
15
ψ (°)

(a)

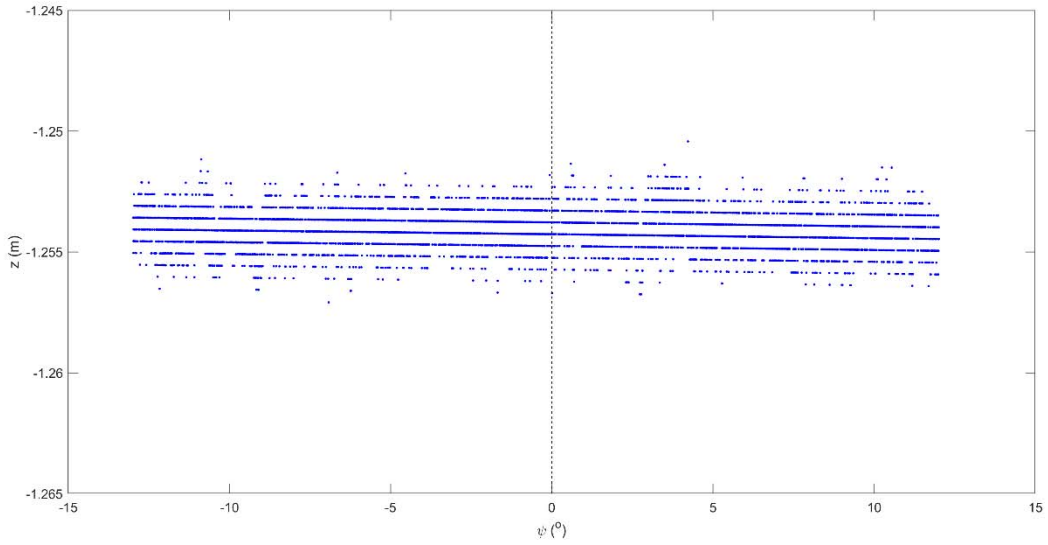
-1.245
-1.25
-1.255
-1.26
-1.265
z (m)
-15
-10
-5
0
5
10
15
ψ (°)

(b)

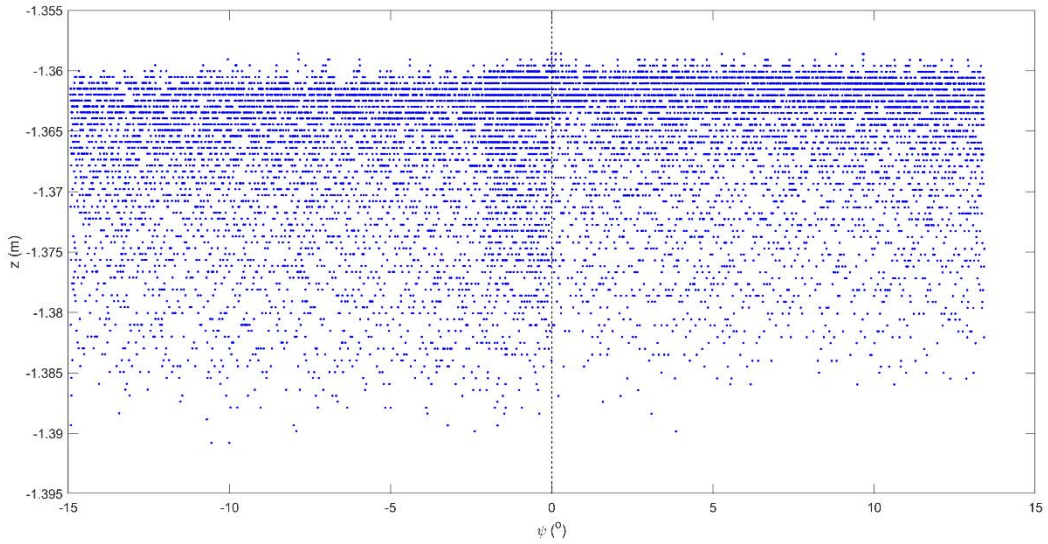
-1.355
-1.36
-1.365
-1.37
-1.375
-1.38
-1.385
-1.39
-1.395
z (m)
-15
-10
-5
0
5
10
15
ψ (°)

(c)

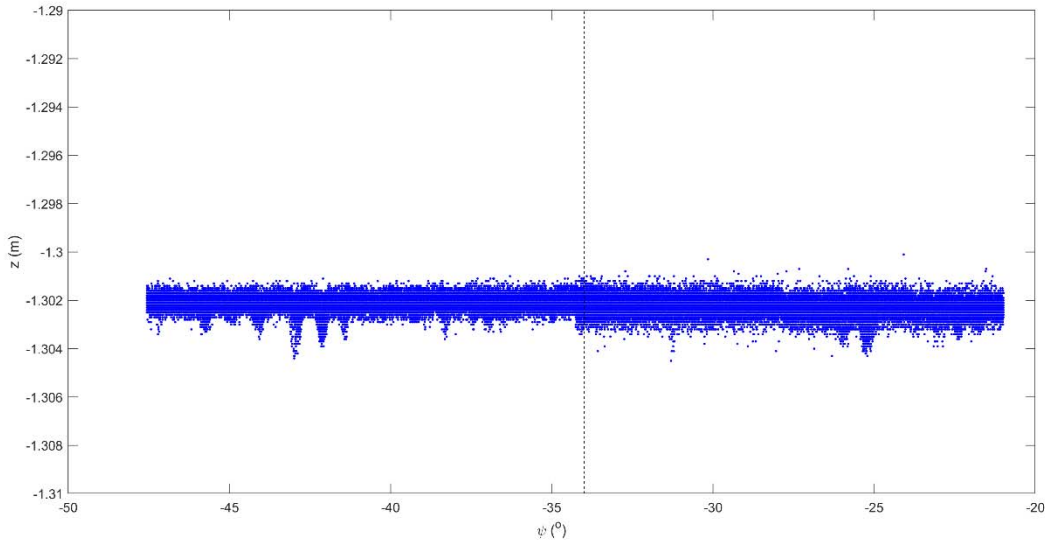
-1.29
-1.292
-1.294
-1.296
-1.298
-1.3
-1.302
-1.304
-1.306
-1.308
-1.31
z (m)
-50
-45
-40
-35
-30
-25
-20
ψ (°)

(d)

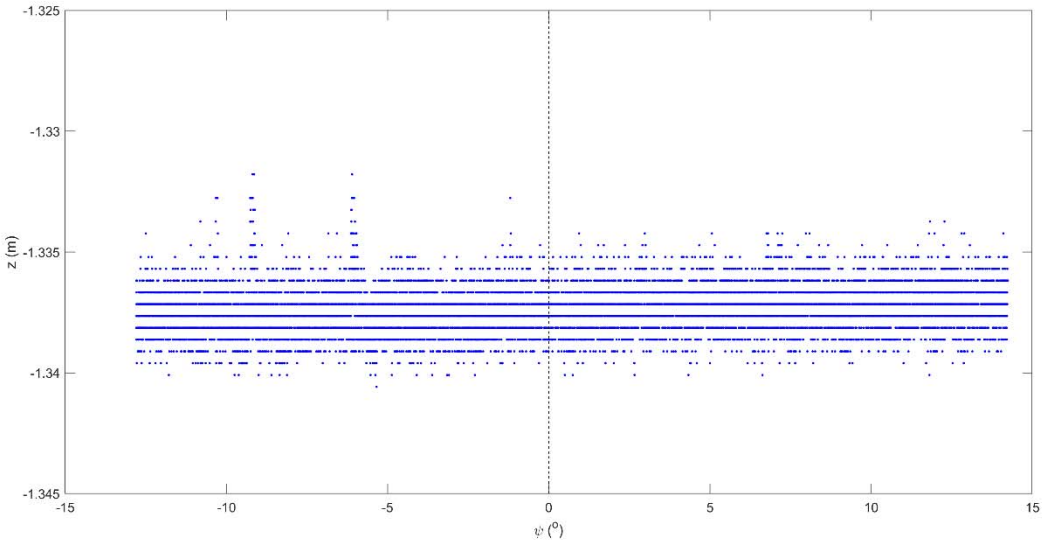
-1.325
-1.33
-1.335
-1.34
-1.345
z (m)
-15
-10
-5
0
5
10
15
ψ (°)

(e)

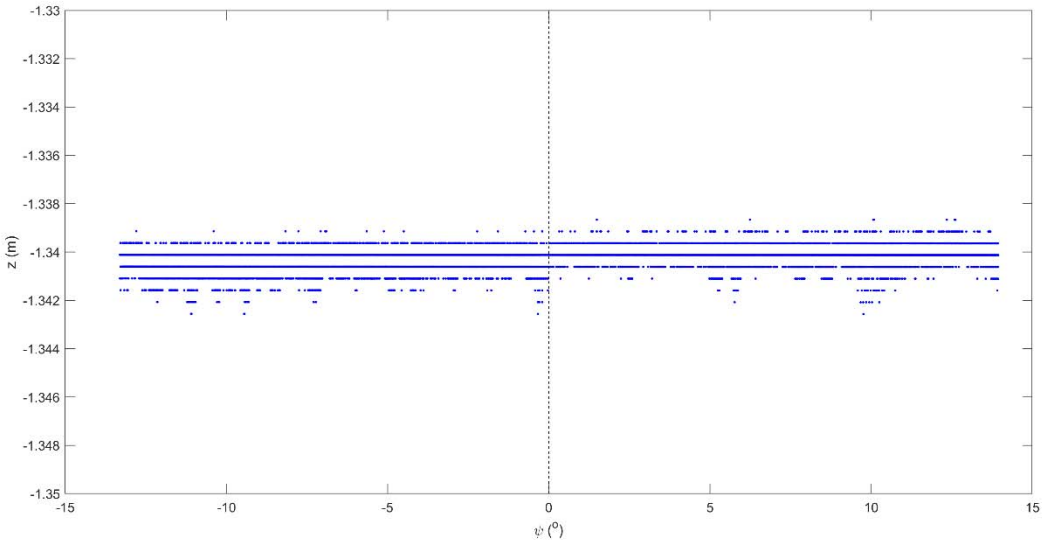
-1.33
-1.332
-1.334
-1.336
-1.338
-1.34
-1.342
-1.344
-1.346
-1.348
-1.35
z (m)
-15
-10
-5
0
5
10
15
ψ (°)

(f)

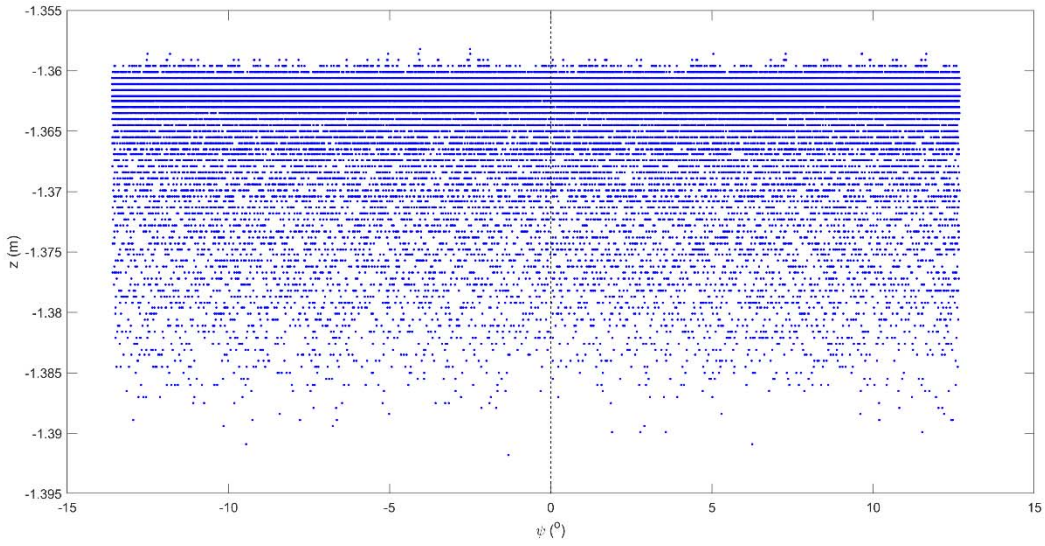

(g)

Fig. 10. Height scan data (Z vs. ψ) at the floor-FoV boundary: a) Faro Focus 3D instrument 1, b) Faro Focus 3D instrument 2, c) Leica HDS6100 (panoramic mode), d) Leica P40, e) Riegl VZ-400, f): Z+F Imager 5010, g) Leica HDS6100 (hybrid mode). The location of the seam line discontinuity is indicated by a dashed vertical line.

4.2 Self-calibration

Stepwise addition of APs resulted in the systematic error models reported in Table 2, with explanations from (Lichti, 2007) provided in Table 3. For each dataset, the estimated residuals for the range, horizontal direction and elevation angle residuals were studied as a function of each observation as well as incidence angle. No un-modelled trends were visible in any of the residual plots after the stepwise model construction. Thus, all instrumental systematic errors were compensated.

Of the APs that were estimated in the self-calibration, the vertical circle index error, and thus the second hypothesis behind the existence of the seam line discontinuities, is of particular interest. The Imager 5010, HDS6100 (panoramic) and P40 calibrations yielded no statistically significant corrections (at the 95% confidence level) for vertical circle index error (c_0). Consequently, as these corrections were not significant, it can be concluded that vertical circle index errors do not contribute to the seam line discontinuity for these sensors. In contrast, however, the c_0 estimates for both Faro Focus 3D scanners were found to be significant. The estimates of c_0 were found to be 27" and 54“, for Faro scanners #1 and #2 respectively. These are, however, smaller in magnitude than what would be necessary in order to

account for the total effect of the seam line discontinuity, which would be errors on the order of 58.5” and 3’16" respectively. The point clouds were also corrected for the estimated systematic errors. Their analysis revealed that the seam line discontinuity was not compensated by the vertical circle index error. Therefore, while the vertical circle index error may be a contributing factor, it can be concluded that it is not the sole cause of the discontinuity observed in the two Faro Focus 3D instruments.

Table 2. Additional parameter models used.

Scanner	**AP model**
Focus 3D #1	$\Delta\rho = a_0 + a_5 \sin\left(\frac{4\pi}{U_2}\rho\right) + a_6 \cos\left(\frac{4\pi}{U_2}\rho\right)$
	$\Delta\theta = b_1 \sec(\alpha) + b_2 \tan(\alpha)$
	$\Delta\alpha = c_0 + c_2 \sin(\alpha)$
Focus 3D #2	$\Delta\rho = a_0$
	$\Delta\theta = b_1 \sec(\alpha) + b_2 \tan(\alpha)$
	$\Delta\alpha = c_0 + c_2 \sin(\alpha)$
HDS6100 (panoramic)	$\Delta\rho = a_0$
	$\Delta\theta = b_3 \sin(2\theta) + b_4 \cos(2\theta)$
	$\Delta\alpha = c_2 \sin(\alpha)$
P40	$\Delta\rho = a_0$
VZ-400	$\Delta\rho = a_0$
	$\Delta\theta = b_3 \sin(2\theta) + b_4 \cos(2\theta)$
Imager 5010	None
HDS6100 (hybrid)	$\Delta\rho = a_0$
	$\Delta\theta = b_3 \sin(2\theta) + b_4 \cos(2\theta)$
	$\Delta\alpha = c_2 \sin(\alpha)$

Table 3. Additional parameter model explanations.

AP(s)	Explanation
a_0	Rangefinder offset error
a_5, a_6	Periodic range errors with wavelength equal to half the second unit length, U_2
b_1	Collimation axis error
b_2	Trunnion axis error
b_3, b_4	Error due to non-orthogonality of the horizontal angle encoder and the vertical axis
c_0	Vertical circle index error
c_2	Vertical circle eccentricity error

The accuracy assessment results are shown in Table 4. The RMS of co-ordinate differences is within millimetre magnitude for all datasets up to the maximum range afforded by the laboratory dimensions. All RMSs differences are of the same order of magnitude of the established target precision and are, therefore, deemed insignificant. Therefore, it can be concluded that no residual systematic error due to the seam line discontinuity is present in the data.

5.0 Conclusions

Several instruments have been tested in a lab environment to identify the cause of and to quantify the so-called seam line discontinuity found in some TLS point clouds. The discontinuity was observed in the data from all five of the panoramic architecture instruments but not in the two hybrid instrument datasets. Three hypotheses for its possible cause were presented. A change in levelling during scanning was eliminated as a possible cause since the data at the lower edge of the FoV did not exhibit the expected pattern and since no change in levelling was observed during the experimental data capture. The vertical circle index error, c_0, was ruled out as the sole cause of the seam line discontinuity for several reasons. First, a statistically significant c_0 was not found for three of the panoramic instruments, including the one showing the largest seam line discontinuity. Second, for the instruments that did possess a statistically significant c_0, the magnitude of this AP was much smaller than the discontinuity.

The most likely cause of the seam line discontinuity is a difference between lower and upper elevation angle scanning limits. This does not introduce a systematic artefact that will affect measurement quality. Rather, it simply limits the data capture taken at extreme elevation angles within the allowable range. This produces the seam line discontinuity as observed due to lost observations at these extreme angles. As such, it has been concluded that notwithstanding any contribution of vertical circle index

effects, as was observed in the two Faro Focus 3D scanners, the effect is of no metric consequence to the final point cloud under the experimental conditions.

Table 4. Accuracy assessment results after self-calibration (Lichti et al., In Press)

	RMS of co-ordinate differences —with APs		
Scanner	**X (mm)**	**Y (mm)**	**Z (mm)**
Focus 3D #1	0.9	0.9	0.3
Focus 3D #2	1.2	1.1	0.4
HDS6100 (panoramic)	0.5	0.5	0.4
P40	0.8	0.7	0.6
VZ-400	0.8	1.0	0.6
Imager 5010	0.9	0.8	0.5
HDS6100 (hybrid)	0.8	0.7	0.6

Acknowledgements

The authors acknowledge funding from the Natural Sciences and Engineering Research Council and the Canada Foundation for Innovation. Spatial Technologies, Calgary, is gratefully acknowledged for the use of the Leica P40. Dr Peter Dawson from the University of Calgary is thanked for the use of the Z+F Imager 5010.

References

Abbas, M.A., Lichti, D.D., Chong, A.K., Setan, H., Majid, Z., 2014. An on-site approach for the self-calibration of terrestrial laser scanner. Measurement 52, 111–123. https://doi.org/10.1016/j.measurement.2014.03.009

Al-Manasir, K., Lichti, D.D., 2015. Self-Calibration of a Lecia HDS7000 Scanner. Presented at the FIG Working Week 2015, Sofia, Bulgaria, p. 12.

Chow, J., Lichti, D., Glennie, C., Hartzell, P., 2013. Improvements to and Comparison of Static Terrestrial LiDAR Self-Calibration Methods. Sensors 13, 7224–7249. https://doi.org/10.3390/s130607224

García-San-Miguel, D., Lerma, J.L., 2013. Geometric calibration of a terrestrial laser scanner with local additional parameters: An automatic strategy. ISPRS Journal of Photogrammetry and Remote Sensing 79, 122–136. https://doi.org/10.1016/j.isprsjprs.2013.02.007

Hartzell, P.J., Gadomski, P.J., Glennie, C.L., Finnegan, D.C., Deems, J.S., 2015. Rigorous error propagation for terrestrial laser scanning with application to snow volume uncertainty. Journal of Glaciology 61, 1147–1158. https://doi.org/10.3189/2015JoG15J031

Kersten, T.P., Mechelke, K., Lindstaedt, M., Sternberg, H., 2009. Methods for Geometric Accuracy Investigations of Terrestrial Laser Scanning Systems. Photogrammetrie - Fernerkundung - Geoinformation 2009, 301–315. https://doi.org/10.1127/1432-8364/2009/0023

Lichti, D.D., 2010. Terrestrial laser scanner self-calibration: Correlation sources and their mitigation. ISPRS Journal of Photogrammetry and Remote Sensing 65, 93–102. https://doi.org/10.1016/j.isprsjprs.2009.09.002

Lichti, D.D., 2007. Error modelling, calibration and analysis of an AM–CW terrestrial laser scanner system. ISPRS Journal of Photogrammetry and Remote Sensing 61, 307–324. https://doi.org/10.1016/j.isprsjprs.2006.10.004

Lichti, D.D., Chow, J., Lahamy, H., 2011. Parameter de-correlation and model-identification in hybrid-style terrestrial laser scanner self-calibration. ISPRS Journal of Photogrammetry and Remote Sensing 66, 317–326. https://doi.org/10.1016/j.isprsjprs.2010.12.001

Lichti, D.D., Glennie, C.L., Jahraus, A., Hartzell, P. (In Press). New approach for low-cost TLS target measurement. ASCE Journal of Surveying Engineering. *Accepted 13/02/2019.*

Medić, T., Christoph Holst, Heiner Kuhlmann, 2017. Towards System Calibration of Panoramic Laser Scanners from a Single Station. Sensors 17, 1145. https://doi.org/10.3390/s17051145

Muralikrishnan, B., Ferrucci, M., Sawyer, D., Gerner, G., Lee, V., Blackburn, C., Phillips, S., Petrov, P., Yakovlev, Y., Astrelin, A., Milligan, S., Palmateer, J., 2015. Volumetric performance evaluation of a laser scanner based on geometric error model. Precision Engineering 40, 139–150. https://doi.org/10.1016/j.precisioneng.2014.11.002

Ogundare, J., 2015. Precision Surveying: The Principles and Geomatics Practice. John Wiley & Sons, Hoboken, NJ.

Reshetyuk, Y., 2010. A unified approach to self-calibration of terrestrial laser scanners. ISPRS Journal of Photogrammetry and Remote Sensing 65, 445–456. https://doi.org/10.1016/j.isprsjprs.2010.05.005

Silvia, E.P., Olsen, M.J., 2012. To Level or Not to Level: Laser Scanner Inclination Sensor Stability and Application. Journal of Surveying Engineering 138, 117–125. https://doi.org/10.1061/(ASCE)SU.1943-5428.0000072

Staiger, R., 2003. Terrestrial Laser Scanning Technology, Systems and Applications. Proceedings of 2nd FIG Regional Conference, Marrakesh, Morocco 10.